Cold Nuclear Matter Effects on Quarkonium Production

R. Vogt

Nuclear and Chemical Sciences Division, Lawrence Livermore National Laboratory, Livermore, CA 94551, USA
Physics and Astronomy Department, University of California, Davis, CA 95616, USA

based on:
RV, Nucl. Phys. A 700 (2002) 539-554
Lourenco, RV, and Wöhri, JHEP 0902 (2009) 014
McGlinchy, Frawley and RV, Phys. Rev. C 87 (2013) 054910

Figure 1: **This work was performed under the auspices of the U.S. Department of Energy by Lawrence Livermore National Laboratory under Contract DE-AC52-07NA27344 and supported by the U.S. Department of Energy, Office of Science, Office of Nuclear Physics (Nuclear Theory) under contract number DE-SC-0004014 and the HEFTY Collaboration.**

Cold Matter Effects on Heavy Flavor Production

Production cross section in a pA collision

$$\sigma_{pA}(S,m^2) \;=\; \sum_{i,j=q,\overline{q},g} \int_{4m_Q^2/S}^{1} \frac{d\tau}{\tau} \int d^2b dz d\epsilon \, dx_1 \, dx_2 \, \delta(x_1x_2-\tau)\delta(x'_F - x_F - \delta x_F(\epsilon))\delta(x'_F - x_1 + x_2)$$
$$\times P(\epsilon) \, S_A^{\rm abs}(\vec{r},z) \, S_{\rm co}(\tau) \, f_i^p(x_1,\mu_F^2,k_T^p) F_i^A(x'_1,\mu_F^2,k_T^A,\vec{b},z) \, \widehat{\sigma}_{ij}(s,m^2,\mu_F^2,\mu_R^2)$$

In AA collisions, the proton PDF would be replaced by that of the nucleus

Survival probability for absorption of a (proto)charmonium state in nuclear matter

$$S_A^{\rm abs}(b,z) = \exp\left\{ - \int_z^\infty dz' \rho_A(b,z')\sigma_{\rm abs}(z-z') \right\}$$

$S^{\rm co}$ **is the survival probability for quarkonium interactions with comovers**

$P(\epsilon)$ **is energy loss probability that modifies the x_F of the produced J/ψ state**

Nuclear parton densities

$$F_i^A(x,Q^2,\vec{b},z) = \rho_A(s) S^i(A,x,Q^2,k_T,\vec{b},z) f_i^p(x,Q^2) \; ; \quad s = \sqrt{b^2+z^2} \; ; \quad \rho_A(s) = \rho_0 \frac{1+\omega(s/R_A)^2}{1+\exp[(s-R_A)/d]}$$

S^i **is shadowing parameterization for parton i**

With no nuclear modifications, $S^i(A,x,Q^2,\vec{r},z) \equiv 1$

The k_T broadening is increased in $p+A$ collisions over $p+p$

Absorption Models, Independent of Other Effects

.

Singlet Absorption Model

All $c\bar{c}$ pairs assumed to be produced in small color singlet states

Assume quadratic growth of cross section with proper time until formation time τ_F (Blaizot and Ollitrault)

Strongest at low to negative x_F where J/ψ can form in the target

Asymptotic ψ' and χ_c cross sections proportional to the final state meson size, *e.g.* $\sigma^{\rm s}_{\psi' N} = \sigma^{\rm s}_{J/\psi N}(r_{\psi'}/r_{J/\psi})^2$ (Povh and Hüfner)

$$\sigma_{\rm abs}(z'-z) = \begin{cases} \sigma^{\rm s}_{CN}\left(\dfrac{\tau}{\tau_F^C}\right)^2 & \textbf{if } \tau < \tau_F^C \\ \sigma^{\rm s}_{CN} & \textbf{otherwise} \end{cases} .$$

$$\begin{aligned} \tau_F^{J/\psi} &= 0.92 \text{ fm} & \sigma^{\rm s}_{J/\psi N} &\sim 2.5 \text{ mb} \\ \tau_F^{\psi'} &= 1.5 \text{ fm} & \sigma^{\rm s}_{\psi' N} &= 3.7\,\sigma^{\rm s}_{J/\psi N} \\ \tau_F^{\chi_c} &= 2 \text{ fm} & \sigma^{\rm s}_{\chi_c N} &= 2.4\,\sigma^{\rm s}_{J/\psi N} \end{aligned}$$

A Dependence of 'Color Transparency'

•

All states produced outside target for $x_F \geq 0$ at 920 GeV (no absorption)

Strong decrease at negative x_F expected in this model for all states but need high statistics to distinguish between them

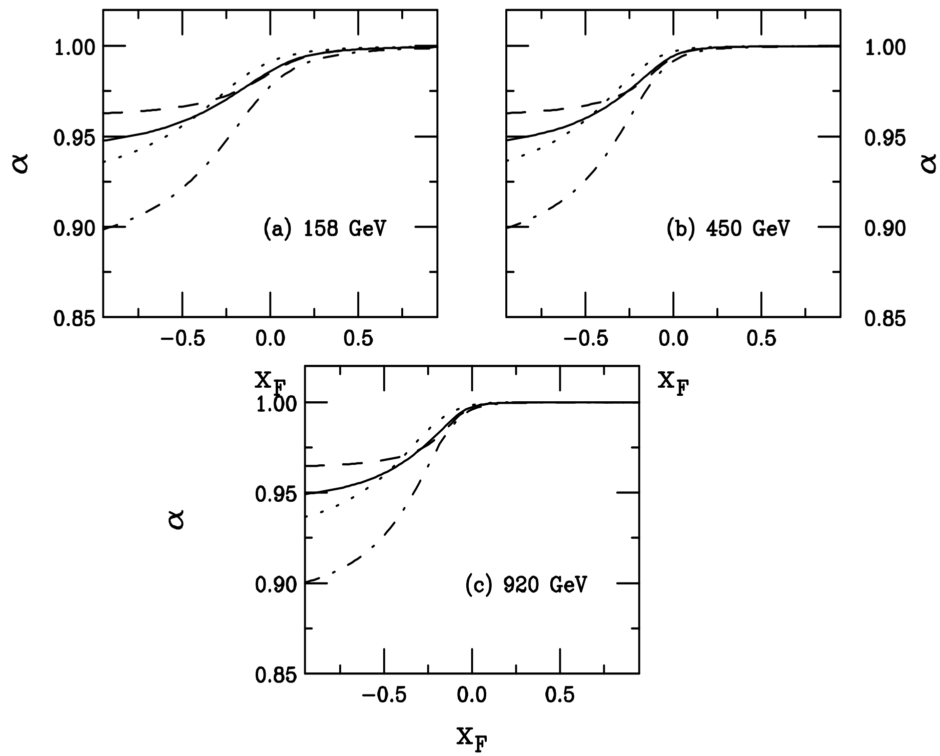

Figure 2: **The A dependence of singlet absorption is shown for 158 (a), 450 (b), and 920 (c) GeV interactions. The total J/ψ (solid), direct J/ψ (dashed), ψ' (dot-dashed) and χ_c (dotted) dependencies are shown. [From R.V., Nucl. Phys. A700 (2002) 539.]**

Octet Absorption Model

Pre-resonant $c\overline{c}$ pairs travel through the nucleus as $|(c\overline{c})_8 g\rangle$ color octet states

Characteristic octet lifetime $\tau_8 \sim 0.25$ fm

For $x_F \geq -0.1$, path length of $|(c\overline{c})_8 g\rangle$ through the target from its production point is greater than maximum path length

These fast states pass through nucleus in color octets so that the pre-resonant A dependence is the same for J/ψ, ψ' and χ_c (Kharzeev and Satz) — $\sigma_{\rm abs}^{\rm o} = 3$ mb agrees with E866 forward A dependence

Universal constant absorption cross section usually assumed for nuclear collision studies (NA38, NA50) where $0 < x_F < 0.18$

At negative x_F, path length is shorter and octet state can neutralize its color inside target and be absorbed as color singlet

Only J/ψ likely to be fully formed inside target even though color neutralization may occur for all states

A Dependence of Octet Absorption

Dependencies different at large negative x_F where neutralization occurs

All values of α identical when state passes through target as octet

As energy increases, color neutralization occurs at more negative x_F

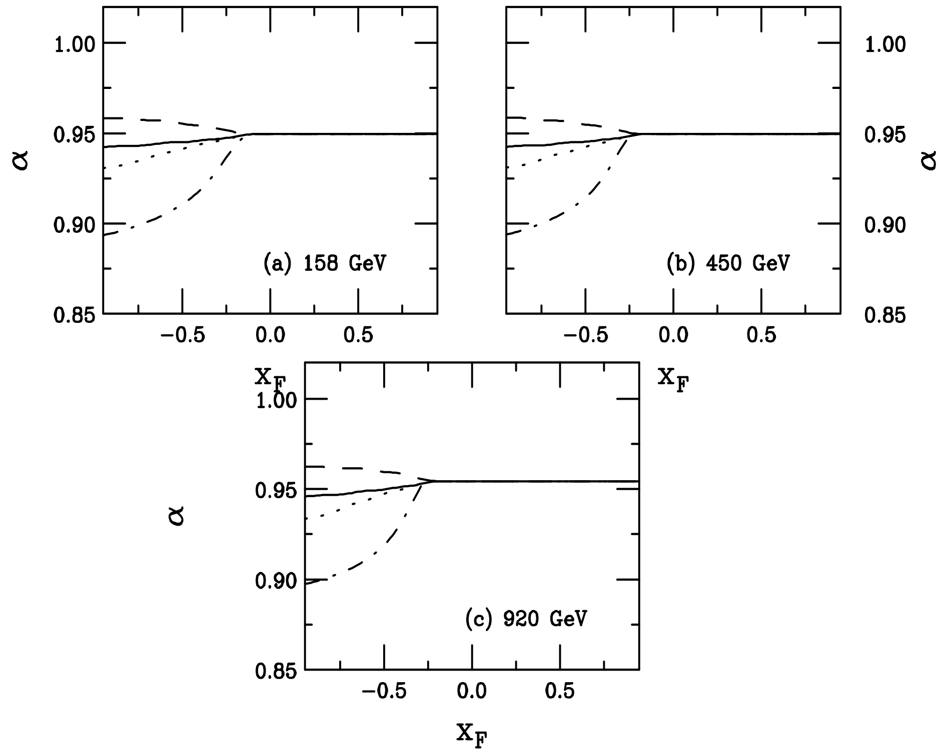

Figure 3: **The A dependence of octet absorption at 158 (a), 450 (b), and 920 (c) GeV interactions. The total J/ψ (solid), direct J/ψ (dashed), ψ' (dot-dashed) and χ_c (dotted) dependencies are shown. [From R.V., Nucl. Phys. A700 (2002) 539.]**

Singlet + Octet Absorption in NRQCD

Relative contributions of singlet and octet production set by NRQCD LDMEs

Equal absorption cross sections for all octet states

Singlet cross sections set by final state size

$$\frac{d\sigma_{pA}^{\psi}}{dx_F} = \int d^2b \left[\frac{d\sigma_{pp}^{\psi,\,\mathrm{oct}}}{dx_F} T_A^{\psi,\mathrm{eff\,(oct)}}(b) + \frac{d\sigma_{pp}^{\psi,\,\mathrm{sing}}}{dx_F} T_A^{\psi,\mathrm{eff\,(sing)}}(b) \right] ,$$

$$\frac{d\sigma_{pA}^{\chi_{cJ}\to J/\psi X}}{dx_F} = \int d^2b \sum_{J=0}^{2} B(\chi_{cJ}\to J/\psi X) \left[\frac{d\sigma_{pp}^{\chi_{cJ},\,\mathrm{oct}}}{dx_F} T_A^{\chi_{cJ},\mathrm{eff\,(oct)}}(b) + \frac{d\sigma_{pp}^{\chi_{cJ},\,\mathrm{sing}}}{dx_F} T_A^{\chi_{cJ},\mathrm{eff\,(sing)}}(b) \right] ,$$

$$\begin{aligned}
\frac{d\sigma_{pA}^{J/\psi,\,\mathrm{tot}}}{dx_F} = \int d^2b \Bigg\{ \Bigg[& \frac{d\sigma_{pp}^{J/\psi,\,\mathrm{dir,\,oct}}}{dx_F} T_A^{J/\psi,\mathrm{eff\,(oct)}}(b) \\
& + \sum_{J=0}^{2} B(\chi_{cJ}\to J/\psi X) \frac{d\sigma_{pp}^{\chi_{cJ},\,\mathrm{oct}}}{dx_F} T_A^{\chi_{cJ},\mathrm{eff\,(oct)}}(b) + B(\psi'\to \psi X) \frac{d\sigma_{pp}^{\psi',\,\mathrm{oct}}}{dx_F} T_A^{\chi_{cJ},\mathrm{eff\,(oct)}}(b) \Bigg] \\
& + \Bigg[\frac{d\sigma_{pp}^{J/\psi,\,\mathrm{dir,\,sing}}}{dx_F} T_A^{J/\psi,\mathrm{dir,eff\,(sing)}}(b) + \sum_{J=0}^{2} B(\chi_{cJ}\to \psi X) \frac{d\sigma_{pp}^{\chi_{cJ},\,\mathrm{sing}}}{dx_F} T_A^{\chi_{cJ},\,\mathrm{eff\,(sing)}}(b) \\
& + B(\psi'\to \psi X) \frac{d\sigma_{pp}^{\psi',\,\mathrm{sing}}}{dx_F} T_A^{\psi',\,\mathrm{eff\,(sing)}}(b) \Bigg] \Bigg\}
\end{aligned}$$

$$T_A^{\mathrm{eff}}(b) = \int_{-\infty}^{\infty} dz\, \rho_A(b,z) \exp\left\{ - \int_z^{\infty} dz' \rho_A(b,z') \sigma_{\mathrm{abs}}(z'-z) \right\}$$

A Dependence of Combination Model

Total J/ψ and ψ' A dependence very similar for $0 < x_F < 0.5$ (previously measured region)

Strong octet component of direct J/ψ makes α nearly constant

Singlet contribution to χ_c means $\alpha \sim 1$ for $0 < x_F < 0.5$

$\alpha(x_F)$ depends on relative octet/singlet contributions

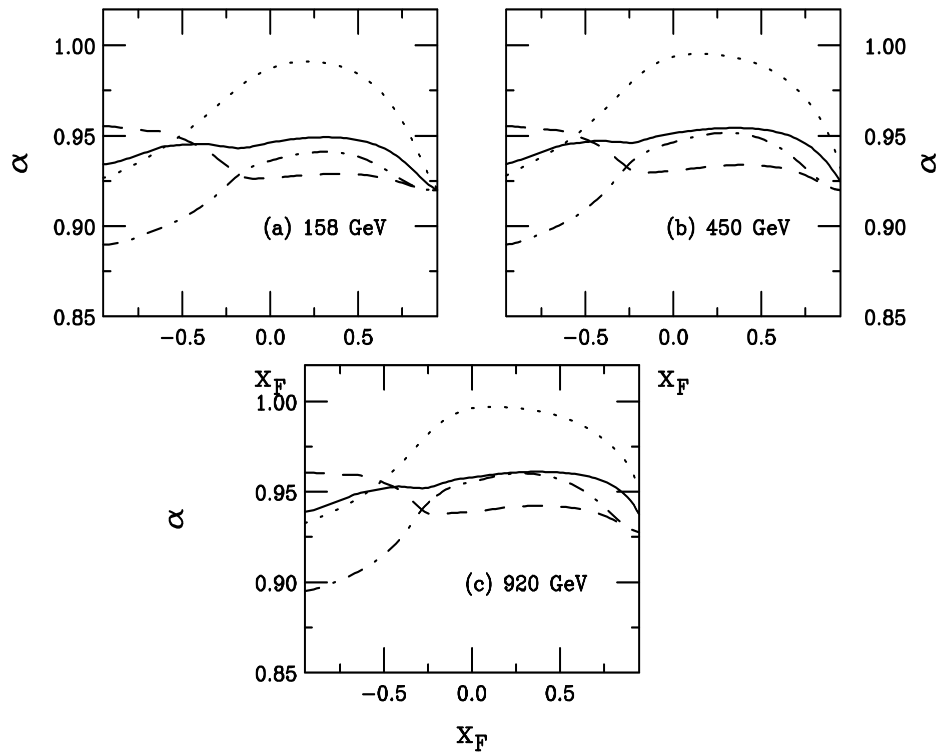

Figure 4: **The A dependence of singlet and octet absorption is shown at 158 (a), 450 (b), and 920 (c) GeV. The total J/ψ (solid), direct J/ψ (dashed), ψ' (dot-dashed) and χ_c (dotted) dependencies are shown. [From R.V., Nucl. Phys. A700 (2002) 539.]**

Absorption with Shadowing

.

Including Absorption with Shadowing at RHIC

Effect of changing $\sigma_{\rm abs}$ is shown for the various absorption models

Little difference between constant and growing octet, only at large negative rapidity, singlet absorption only effective for $y < -2$

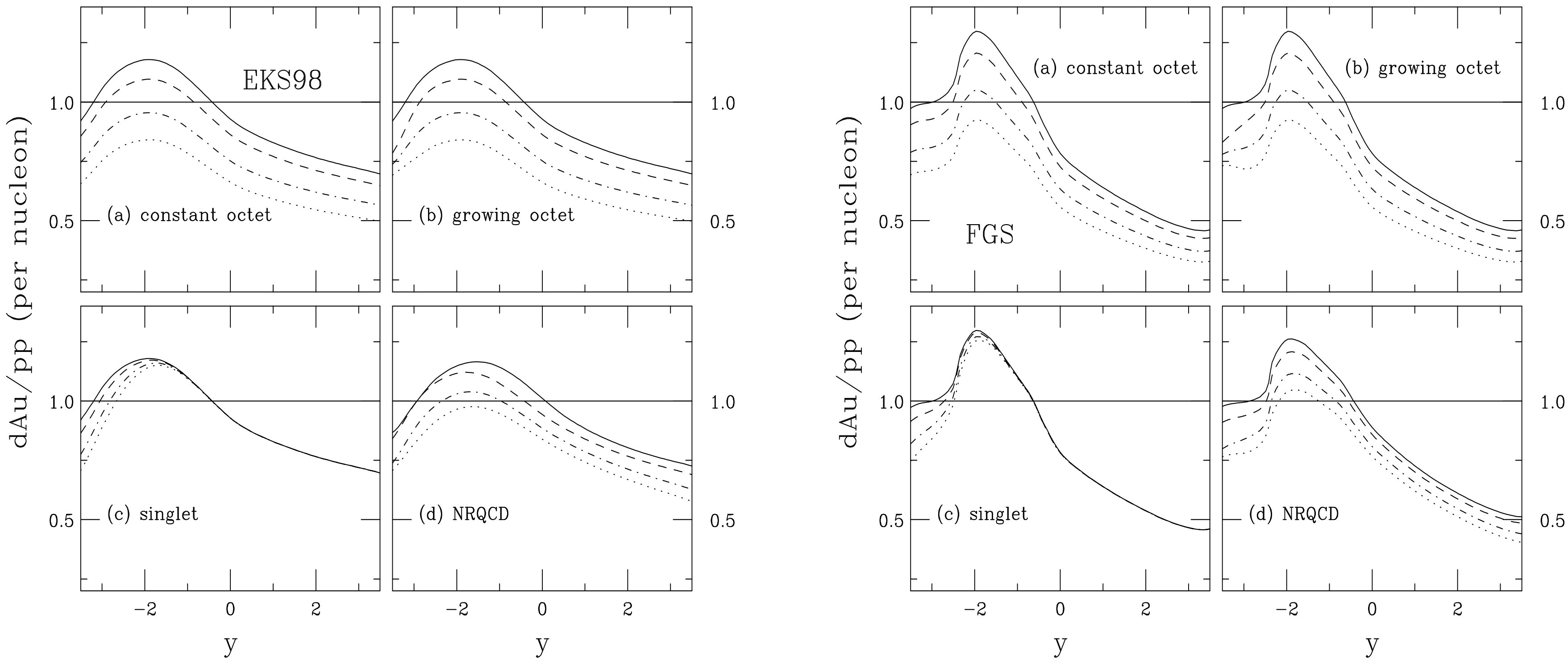

Figure 5: **The J/ψ dAu/pp ratio at 200 GeV with EKS98 (left) and FGS (right) shadowing as a function of rapidity for (a) constant octet (assuming all states have a constant cross section and do not hadronize in the nucleus), (b) growing octet (states behave as singlets if they materialize in the medium), (c) singlet, all calculated in the CEM and (d) NRQCD with a combination of octet and singlet matrix elements. For (a)-(c), the curves are no absorption (solid), $\sigma_{\rm abs} = 1$ (dashed), 3 (dot-dashed) and 5 mb (dotted). For (d), the results are shown for no absorption (solid, note slight difference relative to the CEM), 1 mb octet/1 mb singlet (dashed), 3 mb octet/3 mb singlet (dot-dashed), and 5 mb octet/3 mb singlet (dotted).**

Including Absorption and Shadowing at the LHC

J/ψ not produced inside nucleus except for $y < -5$, no difference between constant and growing octet

Potentially very large J/ψ suppression at $y > -2$, particularly for FGS, even without absorption

.

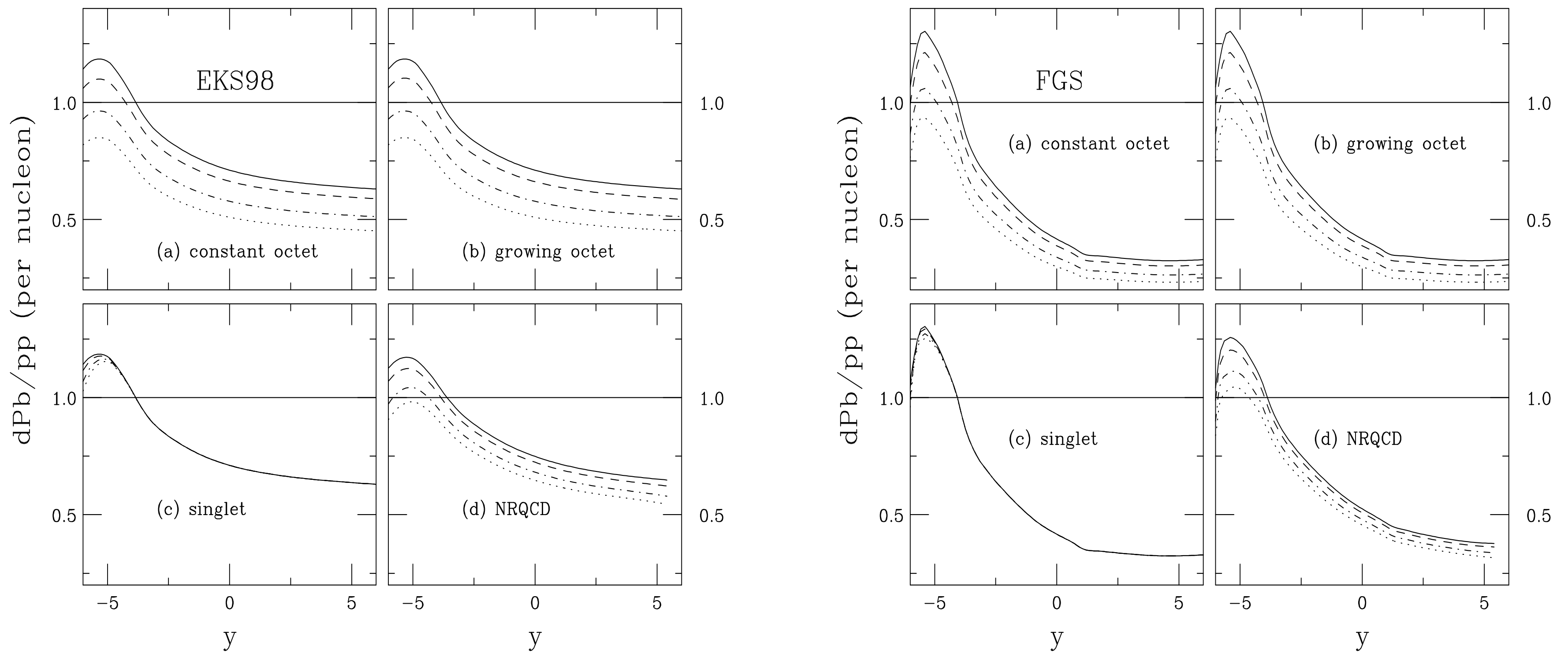

Figure 6: **The J/ψ dAu/pp ratio at 5.5 TeV with EKS98 (left) and FGS (right) shadowing as a function of rapidity for (a) constant octet (assuming all states have a constant cross section and do not hadronize in the nucleus), (b) growing octet (states behave as singlets if they materialize in the medium), (c) singlet, all calculated in the CEM and (d) NRQCD with a combination of octet and singlet matrix elements. For (a)-(c), the curves are no absorption (solid), $\sigma_{\rm abs} = 1$ (dashed), 3 (dot-dashed) and 5 mb (dotted). For (d), the results are shown for no absorption (solid, note slight difference relative to the CEM), 1 mb octet/1 mb singlet (dashed), 3 mb octet/3 mb singlet (dot-dashed), and 5 mb octet/3 mb singlet (dotted).**

Interplay of Shadowing and Absorption

Depending on x values probed, shadowing can enhance or reduce absorption cross section needed to describe data

Absorption alone always gives less than linear A dependence ($\alpha < 1$)

For SPS energies, $17.3 \leq \sqrt{S} \leq 29$ GeV, rapidity range covered is in EMC and antishadowing region, $\alpha > 1$ with no absorption

Adding shadowing to absorption in the SPS energy region requires a larger absorption cross section is needed to maintain agreement with data

For $\sqrt{S} \geq 38$ GeV, x in shadowing regime, thus $\alpha < 1$ with shadowing alone in forward region, reducing needed absorption cross section to $\sigma_{\rm abs} \sim 0$ at the LHC

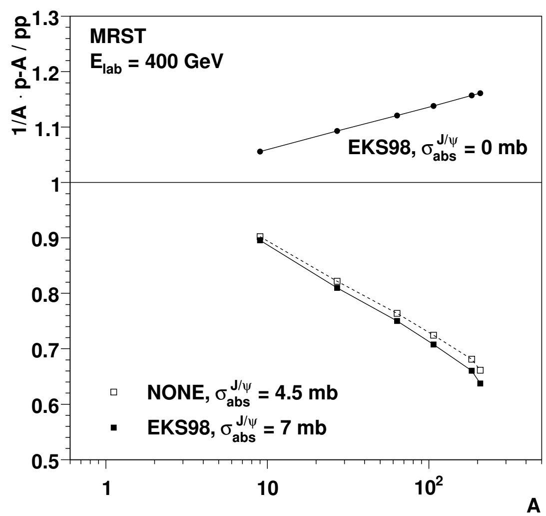

Figure 7: **(Left) Illustration of the interplay between shadowing and absorption. [C. Lourenco, H. K. Woehri and RV, JHEP 0902 (2009) 014.]**

Energy Dependence of $\sigma_{\rm abs}^{J/\psi}$

At midrapidity, systematic decrease of absorption cross section with center of mass energy, independent of shadowing, trend continues at RHIC and above

$\sigma_{\rm abs}^{J/\psi}(y_{\rm cms} = 0)$ **extrapolated to 158 GeV is significantly larger than measured at 450 GeV, underestimating "normal nuclear absorption" in SPS heavy-ion data**

Calculations confirmed by NA60 pA measurements at 158 GeV showing stronger absorption with L

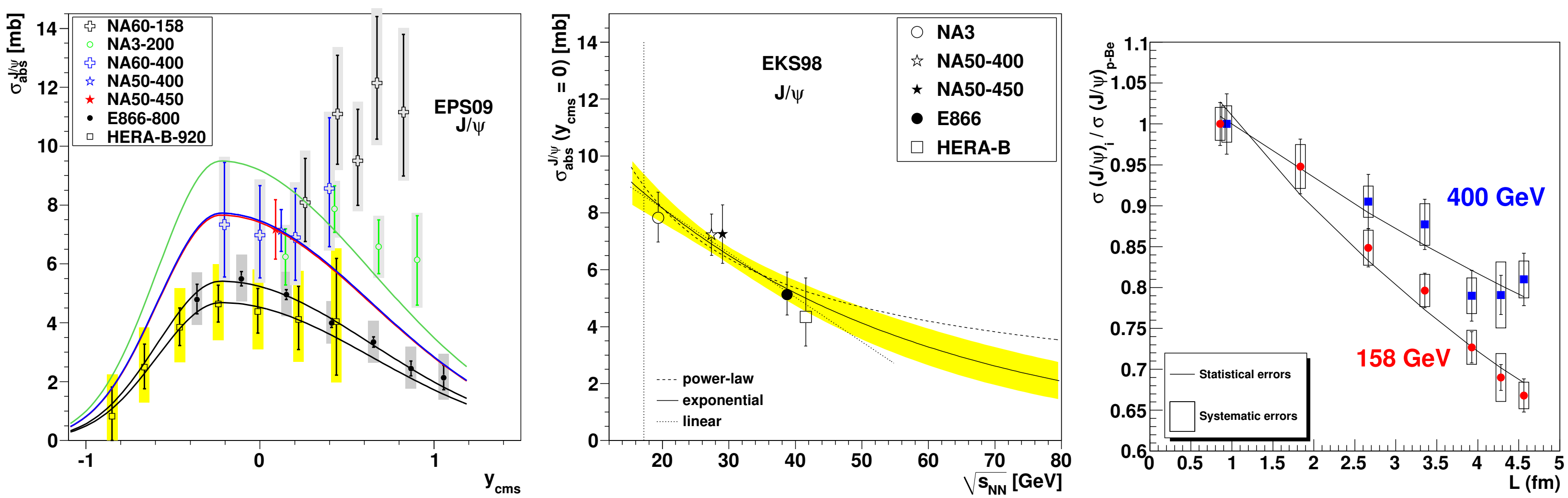

Figure 8: Left: Dependence of $\sigma_{\rm abs}^{J/\psi}$ on $y_{\rm cms}$ for all available data sets including EPS09 shadowing. The shape of the curves is fixed by the E866 and HERA-B data. [Lourenço, RV, Wöhri] Middle: The extracted energy dependence of $\sigma_{\rm abs}^{J/\psi}$ at midrapidity for power law (dashed), exponential (solid) and linear (dotted) approximations to $\sigma_{\rm abs}^{J/\psi}(y = 0, \sqrt{s_{NN}})$ using the EKS98 shadowing parameterization with the CTEQ61L parton densities. The band around the exponential curve indicates the uncertainty in the extracted cross sections at $x_F \sim 0$ from NA3, NA50 at 400 and 450 GeV, E866 and HERA-B. The vertical dotted line indicates the energy of the Pb+Pb and In+In collisions at the CERN SPS. [Lourenço, RV, Wöhri] Right: The J/ψ cross section ratios for pA collisions at 158 GeV (circles) and 400 GeV (squares), as a function of L, the mean thickness of nuclear matter traversed by the J/ψ.

Effective $\sigma_{\rm abs}$ Decreases with $\sqrt{s}$

Once data corrected for shadowing effects, dependence of effective absorption cross section on center of mass energy is visible; should be negligible at LHC energies

In backward region, quarkonium states should be fully formed within the target

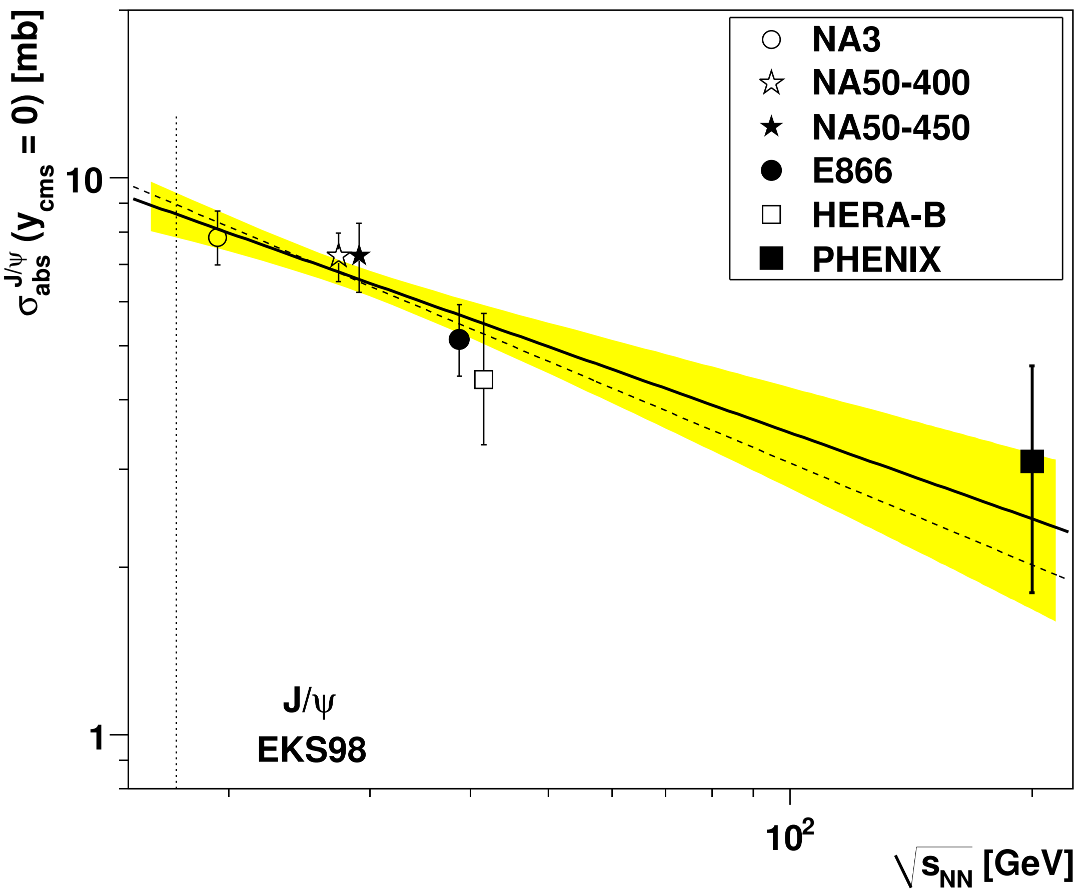

Figure 9: At midrapidity, the effective absorption cross section decreases as a function of energy. (Modified from Lourenco, Wohri and RV.)

$\sigma_{\rm abs}$ Grows with Time $c\bar{c}$ Spends Traversing Nucleus

Mid- and backward rapidity J/ψ at $\sqrt{s_{NN}} = 200$ GeV (longer $\tau = L/\gamma$) dominated by conversion of color octet $c\bar{c}$ pair to color singlet J/ψ by gluon emission

$$\sigma_{\rm abs}(\tau) = \sigma_1 \left(\frac{\sqrt{s}}{10\ GeV}\right)^{0.4} \left(\frac{r_{c\bar{c}}(\tau)}{r_{{\rm J}/\psi}}\right)^2 \qquad r_{c\bar{c}}(\tau) = r_0 + v_{c\bar{c}}\tau \text{ for } r_{c\bar{c}}(\tau) < r_\psi$$

Difference at forward rapidity (shorter τ) where conversion occurs outside target

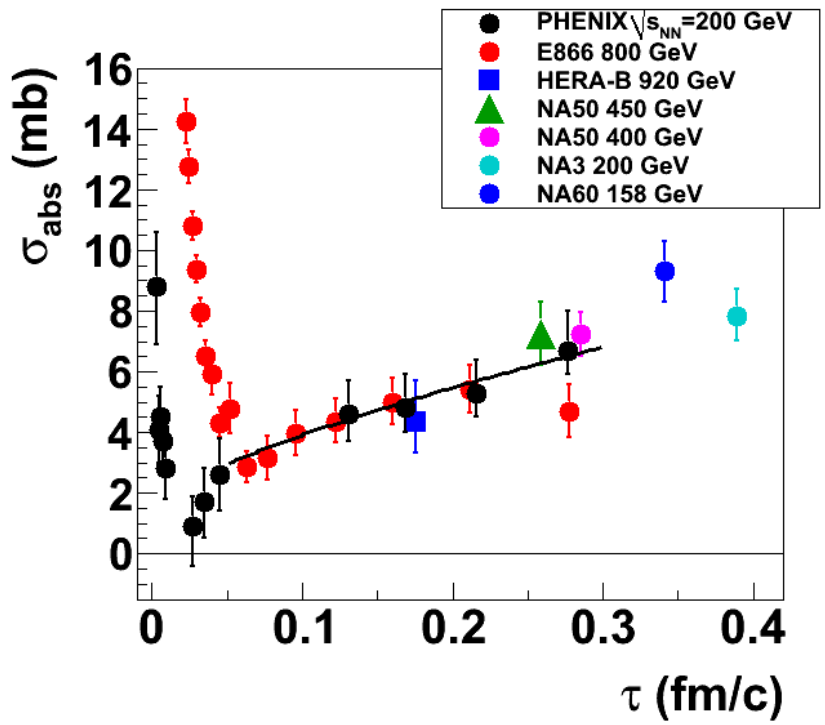

Figure 10: The effective $c\bar{c}$ breakup cross section as a function of the proper time spent in the nucleus, τ. The values were extracted from PHENIX $\sqrt{s_{NN}} = 200$ GeV d+Au data after correction for shadowing using EPS09 and from fixed-target p+A data measured by E866 at 800 GeV, by HERA-B at 920 GeV, by NA50 at 450 GeV and 400 GeV, by NA3 at 200 GeV, and by NA60 at 158 GeV. In all fixed-target cases, the EKS98 parameterization was used. The curve is calculated based on octet-to-singlet conversion inside the nucleus. [D. McGlinchey, A. D. Frawley and RV, Phys. Rev. C **87** (2013) 054910.]

Absorption with Impact Parameter Dependent Shadowing

.

Impact Parameter Dependent Shadowing

.

Impact parameter dependence of shadowing first proposed in Phys. Rev. C 56, 2726 (1997)

Two parameterizations chosen, one with shadowing proportional to the nuclear density and the other proporional to the nuclear thickness at the collision point Both are normalized such that $(1/A)\int d^2b dz \rho(s) S^i(A,x,Q^2,\vec{b},z) = S^i(A,x,Q^2)$

$$S^i_{\rm WS} = S^8(A,x,Q^2,\vec{b},z) = 1 + N_{\rm WS}(S^8(A,x,Q^2)-1)\frac{\rho(\vec{b},z)}{\rho_0}$$

$$S^i_{\rm R}(A,x,Q^2,\vec{b},z) = \begin{cases} 1 + N_{\rm R}(S^i(A,x,Q^2)-1)\sqrt{1-(b/R_A)^2} & b \leq R_A \\ 1 & b > R_A \end{cases} \quad , \tag{1}$$

McGlinchey *et al.* **tried two forms for the impact parameter dependence after these original forms proved too weak for PHENIX d+Au data:**

EPS09s parameterization keeps powers $n = 1 \cdots 4$ **for** A**-independent coefficients**

$$S^i(A,x,Q^2,\vec{b},z) = 1 - (1 - S^i(A,x,Q^2))\left(\frac{T_A^n(b)}{a(n)}\right)$$

Impact parameter dependence assumed to be a step function with radius R **and diffuseness** d **kept as free parameters**

$$S^i(A,x,Q^2,\vec{b},z) = 1 - \left(\frac{1 - S^i(A,x,Q^2)}{a(R,d)(1+\exp((b-R)/d))}\right)$$

Centrality Dependence of CNM on J/ψ in d+Au Collisions

$$\begin{aligned} \text{Path Length Dependence} \quad S^i_\rho(A,x,Q^2,\vec{r},z) &= 1 + N_\rho(S^i(A,x,Q^2)-1)(T_A(\vec{r})/T_A(0))^n \\ \text{Step function Behavior} \quad S^i_\theta(A,x,Q^2,r_T) &= 1 - \left(\frac{1-S^i(A,x,Q^2)}{a(R,d)}\right)/(1+\exp(r_T-R)/d)) \ , \end{aligned}$$

Shadowing appears to be concentrated in core of Au nucleus

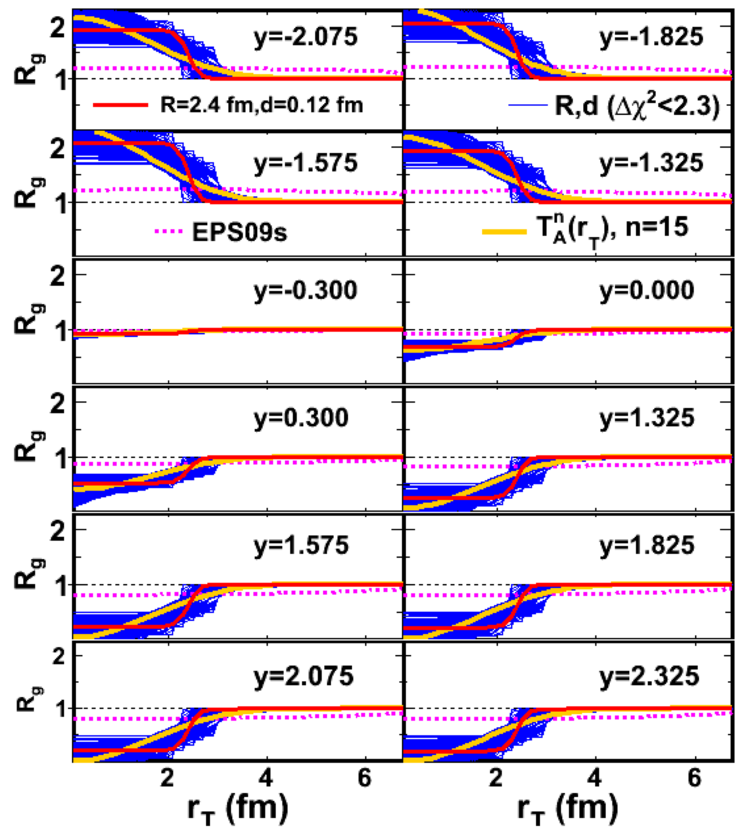

Figure 11: **Transverse radius dependence of gluon shadowing ratio R_g (based on EPS09 NLO) for the PHENIX d+Au rapidity bins. The results compare b-dependence based on path length through the nucleus, $T_A(b)$, and a sharp surface with radius and diffuseness parameters.**

Dependence of $\sigma_{\rm abs}$ on Rapidity and Nuclear Gluon Density

Effective $\sigma_{\rm abs}$ is a function of rapidity, essentially independent of centrality, exponential absorption has significantly different centrality dependence than shadowing

Forward rise could be due to energy loss effects at larger x_F; backward enhancement in $\sigma_{\rm abs}$ could be related to formation time effects

Smaller difference between EPS09s and ALICE data at the LHC, likely shadowing occurs over more of the nuclear profile, not just the core, at higher energy

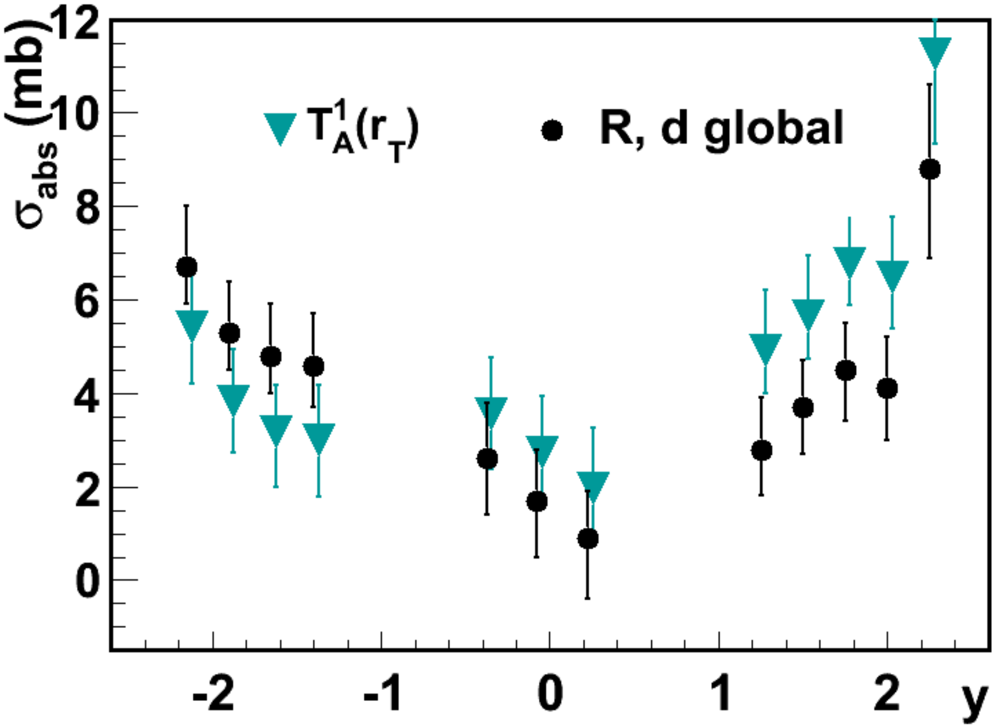

Figure 12: **The rapidity dependence of $\sigma_{\rm abs}$ for two assumptions about shadowing centrality dependence.** (**McGlinchey** *et al.*)

Briefly: Comover Interaction Model

.

Comover Interaction Model, Ferriero *et al.*

Comover interaction rate

$$\Gamma^{\mathcal{Q}}(T) = \int_{E^{\mathcal{Q}}_{\rm thr}}^{\infty} dE^{\rm co}\, \sigma^{\mathcal{Q}}_{\rm geo} \left(1 - \frac{E^{\mathcal{Q}}_{\rm thr}}{E^{\rm co}}\right)^n \frac{\rho^{\rm co}}{e^{E^{\rm co}/T_{\rm eff}} - 1} \tag{2}$$

$E^Q_{\rm thr} = M_Q + m_{\rm co} - 2M_H$ **where** $Q = c$ **or** b**,** $H = D$ **or** B**,** $E^{\rm co} = \sqrt{p^2 + m^2_{\rm co}}$ **with** $m_{\rm co} = 0$ **for gluons and 140 MeV for pions;** ρ^0 **is the transverse density of comovers, proportional to the multiplicities;** $\sigma^0_{\rm geo} \simeq \pi r^2_Q$**; the power** n **is between 0.5 and 2 and** $T_{\rm eff} \simeq 200 - 300$ **MeV**

Dissociation of quarkonium by comover interactions as a function of time

$$\tau \frac{\mathbf{d}\rho^{\mathcal{Q}}}{\mathbf{d}\tau}\,(b,s,y) \;=\; -\sigma^{\rm co-\mathcal{Q}}\, \rho^{\rm co}(b,s,y)\, \rho^{\mathcal{Q}}(b,s,y)\;, \tag{3}$$

$\sigma^{\rm co-Q}$ **is the energy-averaged quarkonium-comover interaction cross section**

The densities of comovers and quarkonium are $\rho^{\rm co}$ **and** ρ^Q **respectively**

Integrating over time τ **from** τ_i **to** τ_f **gives the survival probability**

$$S^{\rm co}_{\mathcal{Q}}(b,s,y) \;=\; \exp\left\{ -\,\sigma^{\rm co-\mathcal{Q}}\, \rho^{\rm co}(b,s,y)\, \ln\left(\rho^{\rm co}(b,s,y)/\rho_{pp}(y)\right)\right\} \tag{4}$$

Shadowing is included but other cold matter effects are not

The different sizes of $\sigma^{\rm co-Q}$ **for** $Q = J/\psi$ **and** ψ**(2S) result in stronger comover dissociation for** ψ' **than** J/ψ

It has been shown that the A **dependence of comover interactions and nucleon absorption are effectively the same (Gavin and Vogt)**

Comover Effects on Charmonium at the LHC

$\sigma^{\mathrm{co}-Q}$ **was fixed to fits to low-energy experimental data to be** $\sigma^{\mathrm{co}-J/\psi} = 0.65$ **mb for the** J/ψ **and** $\sigma^{\mathrm{co}-\psi(2\mathrm{S})} = 6$ **mb for the** ψ**(2S)**

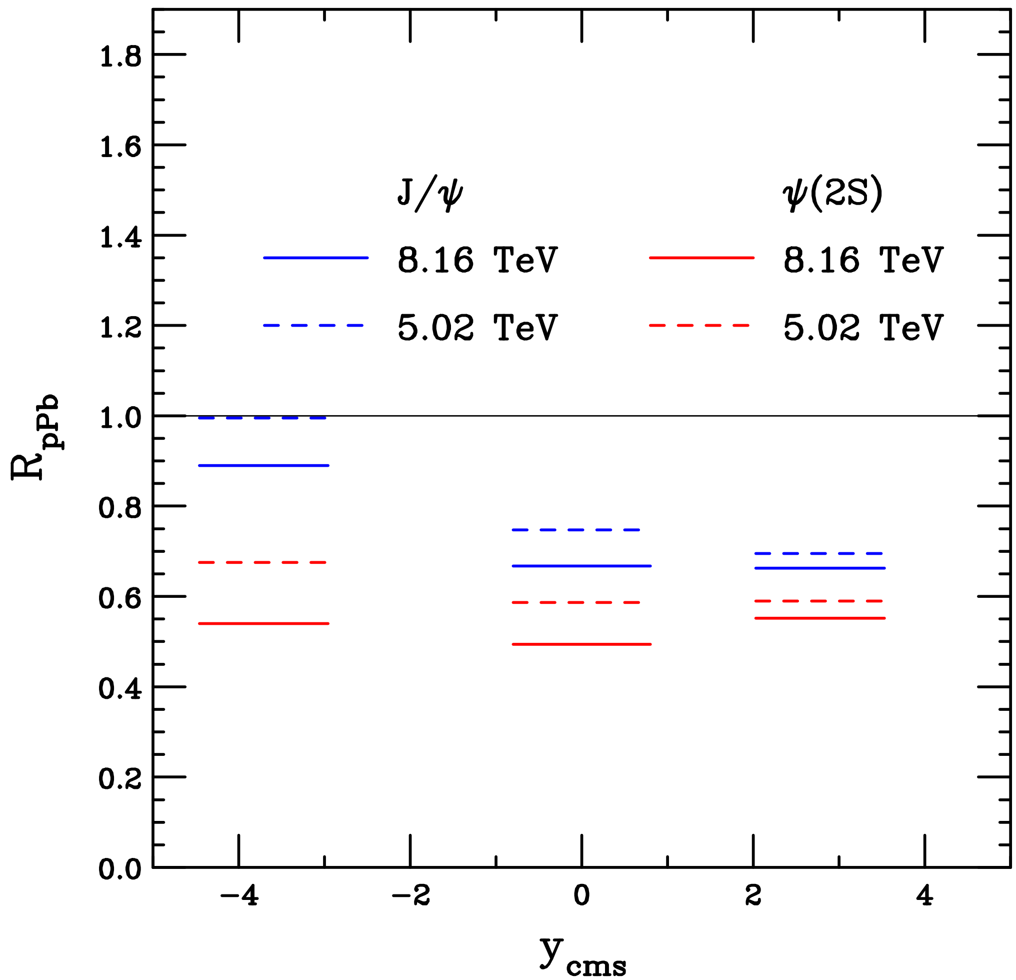

Figure 13: **The rapidity dependence of** J/ψ **and** ψ**(2S) production in the comover interaction model compared between 5.02 and 8.16 TeV, from Elena Ferreiro.**

J/ψ Production by Intrinsic Charm

.

What is Intrinsic Charm?

Proton wavefunction can be expanded as sum over complete basis of quark and gluon states: $|\Psi_p\rangle = \sum_m |m\rangle\, \psi_{m/p}(x_i, k_{T,i}, \lambda_i)$

$|m\rangle$ **are color singlet state fluctuations into Fock components** $|uud\rangle$, $|uudg\rangle \cdots |uudc\overline{c}\rangle$

The intrinsic charm fluctuations can be freed by a soft interaction if the system is probed during the time $\Delta t = 2p_{\rm lab}/M^2_{c\overline{c}}$ **that the fluctuations exist**

Dominant Fock state configurations have minimal invariant mass, $M^2 = \sum_i m^2_{T,i}/x_i$**, where** $m^2_{T,i} = k^2_{T,i} + m^2_i$ **is the squared transverse mass of parton** i **in the state; corresponds to configurations with equal rapidity constituents**

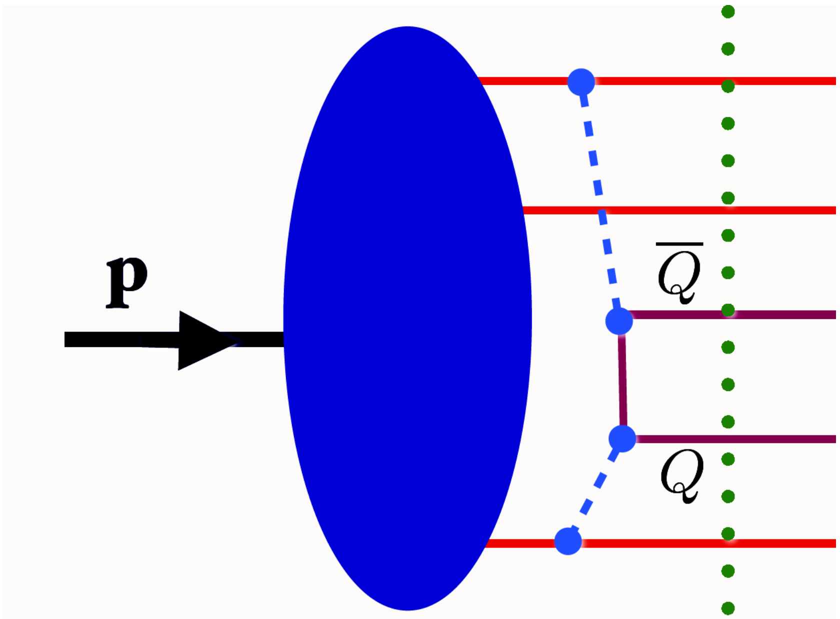

Intrinsic Charm is a Long-Standing Puzzle in QCD

Intrinsic charm in the proton $|uudc\bar{c}\rangle$, was first proposed in the 1980's

If this state dominates the wavefunction, the charm quarks carry a larger fraction of the hadron momentum, enhancing charm production in the forward x_F region

A number of experimental hints have been seen, no conclusive results

- **Charm structure function, F_2^c, large at largest x and highest Q^2 measured (EMC)**
- **Leading charm asymmetries consistent with intrinsic charm predictions (D^- over D^+ in $\pi^- p$ interactions, E791)**
- **Double J/ψ production observed at high pair x_F by NA3**
- **Forward charm production observed in many fixed-target experiments (WA82, WA89, E791, SELEX and others)**
- **Proposed explanation of high energy astrophysical neutrino rate at Ice Cube (Brodsky and Laha)**
- **LHCb $Z+c$-jet measurements at forward rapidity consistent with intrinsic charm**

Global PDF analyses have tried incorporating intrinsic charm and reported a range of possible contributions from 0 to 1%, most lately the NNPDF Collaboration (Nature) and the CTEQ Collaboration

At colliders, intrinsic charm is boosted to high rapidity and detection is less likely, fixed-target configurations may be better for discovery measurement

Heavy Flavor Production by Intrinsic Charm

Probability distribution of five-particle Fock state of the proton:

$$dP_{\mathrm{ic}\,5} = P^0_{\mathrm{ic}\,5} N_5 \int dx_1 \cdots dx_5 \int dk_{x\,1} \cdots dk_{x\,5} \int dk_{y\,1} \cdots dk_{y\,5} \frac{\delta(1 - \sum_{i=1}^5 x_i)\delta(\sum_{i=1}^5 k_{x\,i})\delta(\sum_{i=1}^5 k_{y\,i})}{(m_p^2 - \sum_{i=1}^5 (\widehat{m}_i^2/x_i))^2}$$

$i = 1, 2, 3$ **are** u, u, d **light quarks, 4 and 5 are** c **and** $\overline{c}$**,** N_t **normalizes the probability to unity and** P^0_{ic} **scales the normalized probability to the assumed intrinsic charm content: 0.1%, 0.31% and 1% are used to represent the range of probabilities assumed previously (based on original Brodsky** *et al.* **model**

The IC cross section is determined from soft interaction scale breaking coherence of the Fock state, $\mu^2 = 0.1$ **GeV**^{2}

$$\sigma_{\mathrm{ic}}(pp) = P_{\mathrm{ic}\,5} \sigma^{\mathrm{in}}_{pN} \frac{\mu^2}{4\widehat{m}_c^2}$$

The cross sections from intrinsic charm are then obtained by multiplying by the normalization factor for the CEM to the J/ψ

$$\sigma^{J/\psi}_{\mathrm{ic}}(pp) = F_C \sigma_{\mathrm{ic}}(pp)$$

The A **dependence is the same for both** $\overline{D}$ **and** J/ψ

$$\sigma_{\mathrm{ic}}(pA) = \sigma_{\mathrm{ic}}(pp)\, A^\beta \quad , \beta = 0.71 \ \ (\mathrm{NA3})$$

Other assumptions of intrinsic charm distributions in the nucleon are the meson cloud model ($c(x) \neq \overline{c}(x)$**) and a sea-like distribution (**$c(x) = \overline{c}(x) \propto \overline{d}(x) + \overline{u}(x)$**)**

Combining Perturbative Charm with IC

The production cross sections are calculated with a combination of perturbative QCD and intrinsic charm contributions; in $p + p$ collisions:

$$\sigma_{pp}^{J/\psi} = \sigma_{\rm CEM}(pp) + \sigma_{\rm ic}^{J/\psi}(pp)$$

The J/ψ cross sections are computed at NLO in the color evaporation model for $p + p$ and $p + A$ interactions; $\sigma_{\rm ic}$ is the intrinsic charm cross section using Brodsky *et al.* "flavor" of IC

In $p + A$ collisions:

$$\sigma_{pA}^{J/\psi} = \sigma_{\rm CEM}(pA) + \sigma_{\rm ic}^{J/\psi}(pA)$$

The CEM calculation in $p + A$ collisions include k_T broadening, shadowing, and absorption

Summary of Previous Fixed-Target J/ψ Data

NA60 $p_{\rm lab} = 158$ **and 400 GeV, covering** $0.05 < x_F < 0.4$ **and** $-0.075 < x_F < 0.125$ **respectively, were taken on Be, Al, Cu, In, W, Pb, and U targets (PLB 706, 263 (2012))**

NA3 $p_{\rm lab} = 200$ **GeV,** $x_F > 0$**, taken on a Pt target (Z. Phys. C 20, 101 (1983))**

NA50 $p_{\rm lab} = 450$ **GeV, midrapidity (**$-0.1 < x_F < 0.1$**), used Be, Al, Cu, Ag, W and Pb targets (EPJ C 33, 31 (2004))**

E866 $p_{\rm lab} = 800$ **GeV,** $-0.09 < x_F < 0.95$**, used Be, Fe, and W targets (PRL 84, 3256 (2000))**

HERA-B $p_{\rm lab} = 920$ **GeV,** $-0.34 < x_F < 0.14$**, used C, Ti and W targets (EPJ C 60, 525 (2009))**

E866 J/ψ x_F and p_T Distributions $(p + p)$

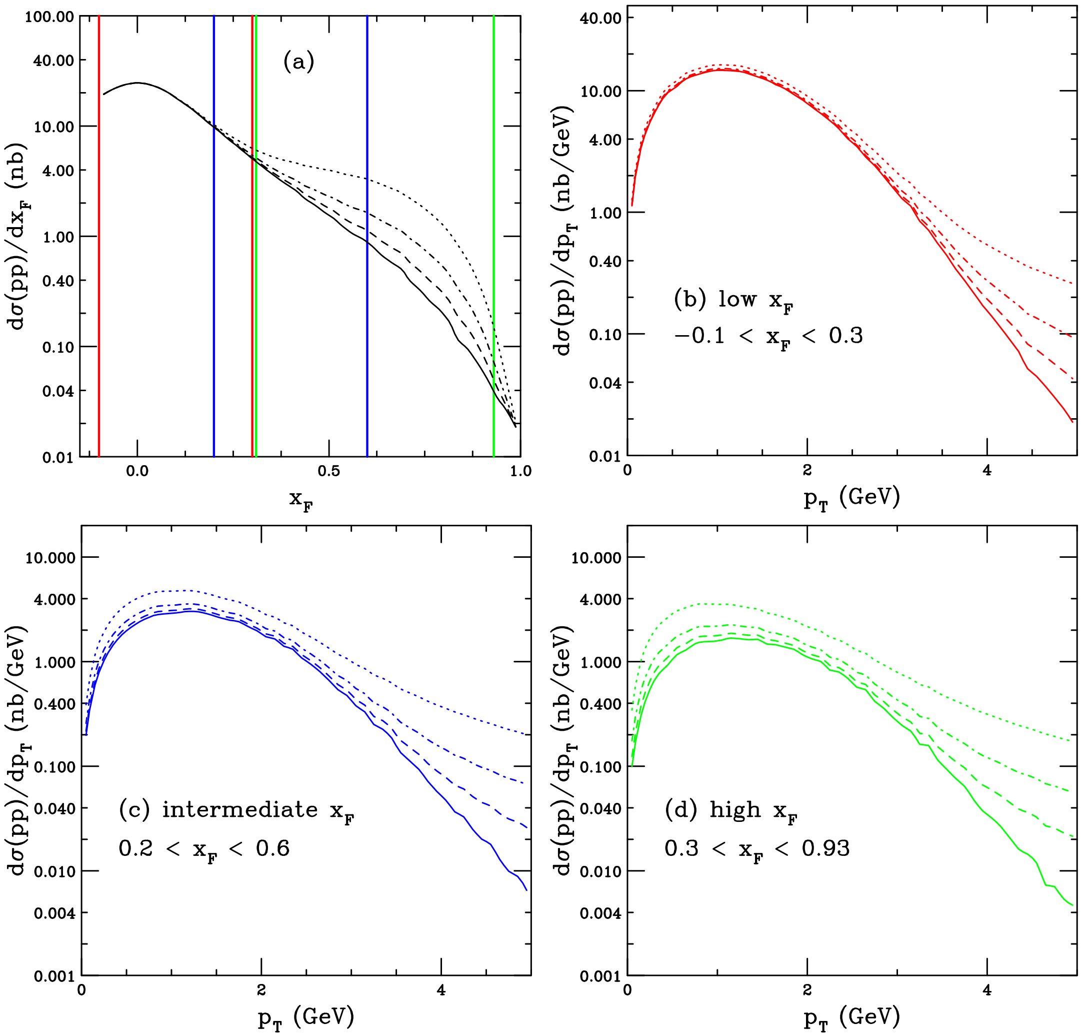

Figure 14: The J/ψ cross sections in $p+p$ collisions at $\sqrt{s} = 38.8$ GeV with and without IC as a function of x_F (a) and p_T at low (b), intermediate (c), and high x_F (d). The solid curves do not include IC while the dashed, dot-dashed and dotted curves use $P^0_{\mathrm{ic}\,5} = 0.1\%$, 0.31% and 1% respectively. The colored vertical bars on the x_F distributions show the x_F limits of the p_T distributions in (b)-(d) and matches the color of the curves in (b)-(d). RV, PRC **103**, 035204 (2021).

Comparison with α Extracted from E866 J/ψ $p + A$ Data

E866 obtained α as a function of x_F and p_T (in 3 x_F bins) for $A = \mathrm{Be}$, Fe, and W

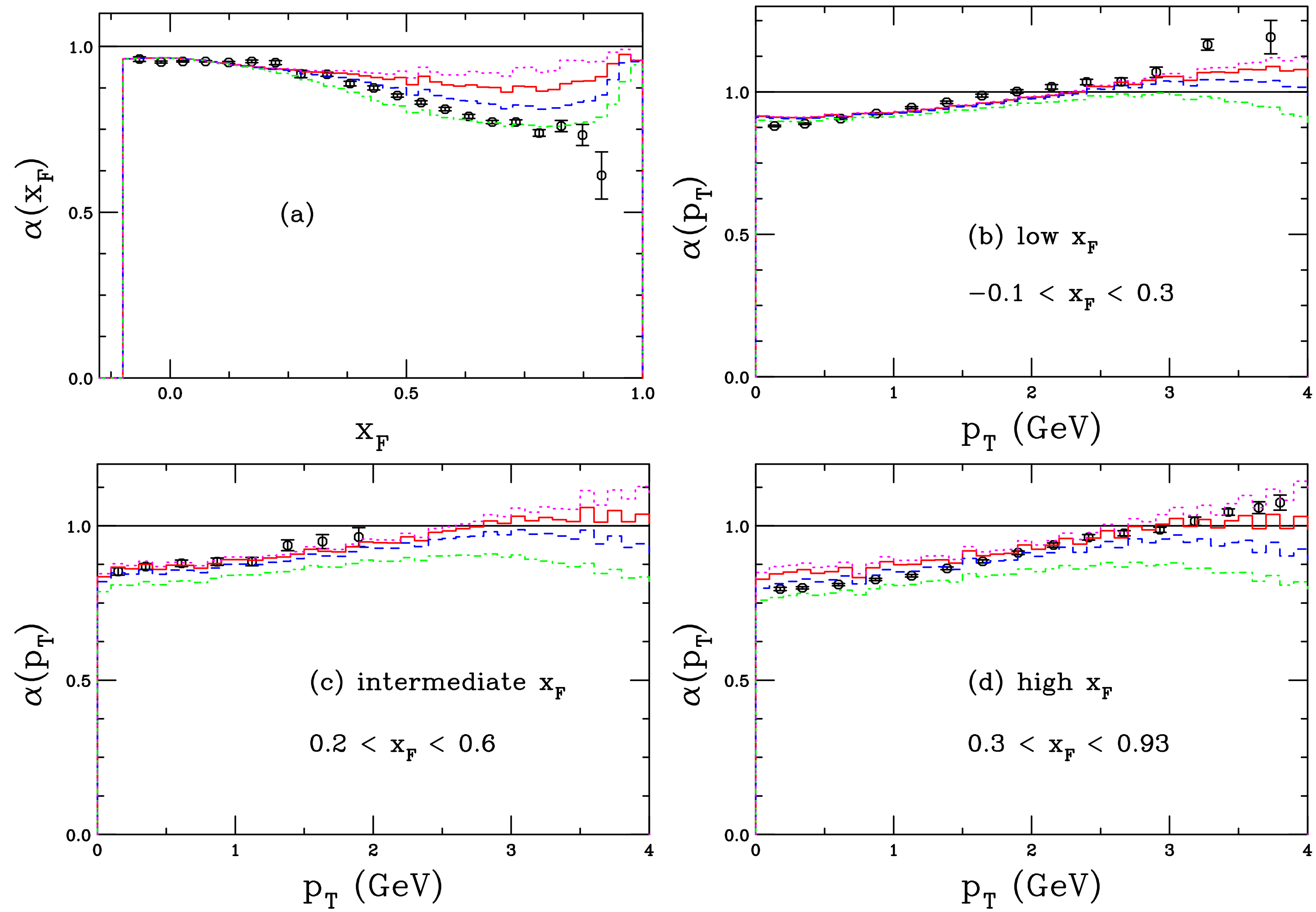

Figure 15: The exponent $\alpha(x_F)$ (a) and $\alpha(p_T)$ for low x_F (b), intermediate x_F (c), and high x_F (d). The dotted magenta curves use $P^0_{\rm ic\,5} = 0$ while the solid red, dashed blue, and dot-dashed green curves show $P^0_{\rm ic\,5} = 0.1\%$, 0.31% and 1% respectively. The E866 data (PRL **84**, 3256 (2000)) are the black points. From: RV, PRC **103**, 035204 (2021).

Comparison of $\alpha(x_F)$ with Fixed-Target J/ψ Data

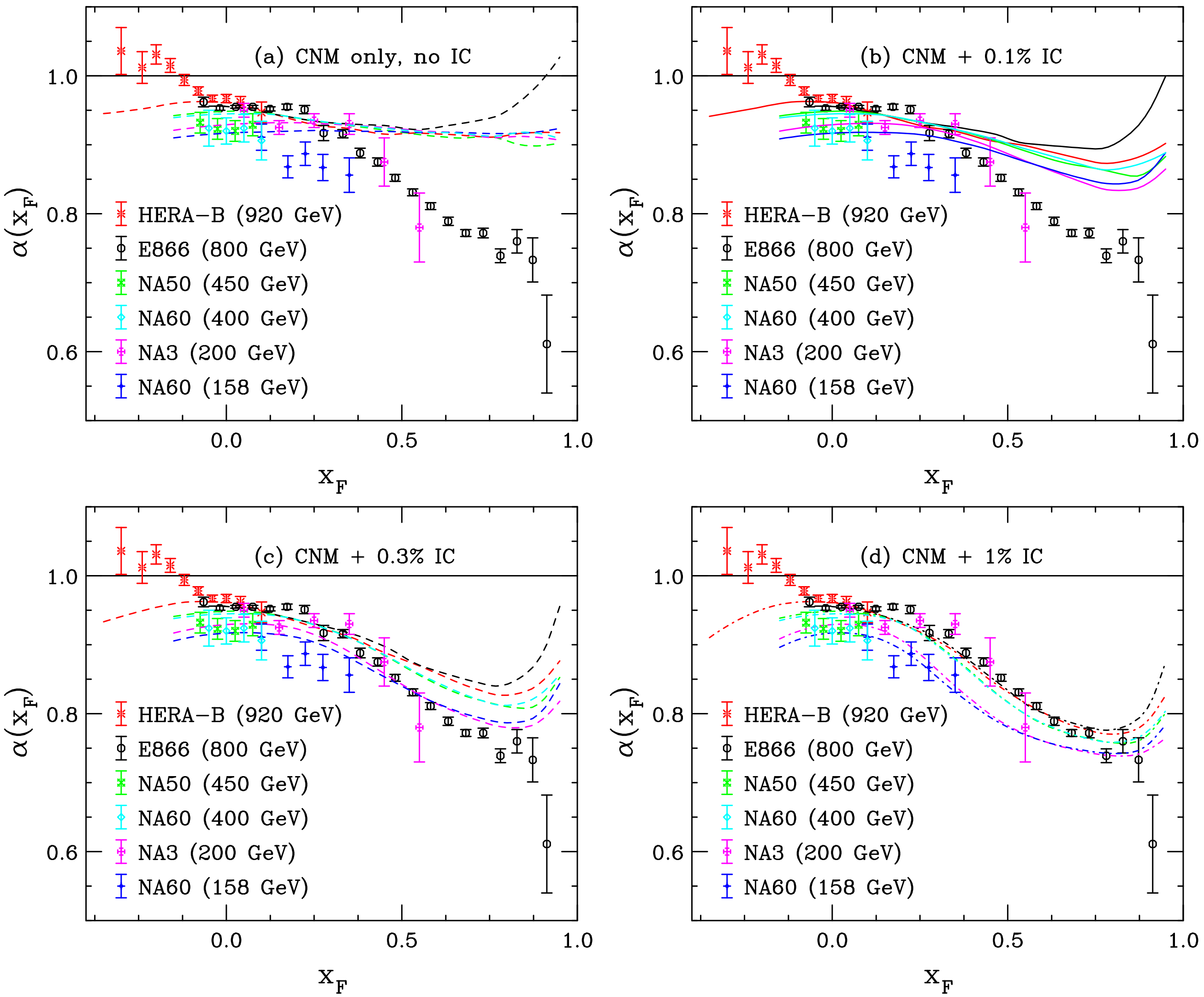

Figure 16: The value of $\alpha(x_F)$ for J/ψ production at: NA60 ($p_{\rm lab} = 158$ GeV), NA3 ($p_{\rm lab} = 200$ GeV), NA60 ($p_{\rm lab} = 400$ GeV), NA50 ($p_{\rm lab} = 450$ GeV), E866 ($p_{\rm lab} = 800$ GeV), and HERA-B ($p_{\rm lab} = 920$ GeV). The points and curves of the same color are at the same energy. Calculations with $P^0_{{\rm ic}\,5} = 0$ are in (a) while $P^0_{{\rm ic}\,5} = 0.1\%$, 0.3%, and 1% are shown in (b)-(d).

Recent and Forthcoming Fixed-Target Experiments Ideal for IC Studies

Many previous experiments studied J/ψ production off nuclear targets at proton beam energies from 158 to 920 GeV, several used to get a baseline for $A+A$ collisions; those that covered large x_F saw a larger suppression of production off nuclear targets at higher x_F

SeaQuest: Took data with a 120 GeV proton beam on p, d, C, Fe, and W targets, covered forward region, $0.4 < x_F < 0.95$ and $p_T < 2.3$ GeV; J/ψ data not published yet but should report nuclear suppression factor, $pA/p\mathrm{d}$

SMOG: Gas jet target in LHCb, J/ψ and D^0 measured at backward rapidity in the fixed-target center of mass, data so far at: $p + \mathrm{Ne}$ at $\sqrt{s_{NN}} = 68.5$ GeV; $p + \mathrm{He}$ at $\sqrt{s_{NN}} = 86.6$ GeV; and $p + \mathrm{Ar}$ at $\sqrt{s_{NN}} = 110.4$ GeV

NA60+: proton beams at $p_{\mathrm{lab}} = 40$, 80, and 120 GeV, nuclear targets from Be to Pb

Calculations and comparison to data in the following from R. Vogt, arXiv:2101.02858, Phys. Rev. C 103, 035204 (2021); arXiv:2207.04347, Phys. Rev. C 106, 025201 (2022); arXiv:2304.03451, Phys. Rev. C 108, 015201 (2023)

SeaQuest Results for $p + \mathrm{W}$ Interactions

The large x_F contribution from intrinsic charm changes the x_F dependence from effectively flat to decreasing with x_F

Enhanced k_T broadening evident with no intrinsic charm, effect is reduced when IC is included

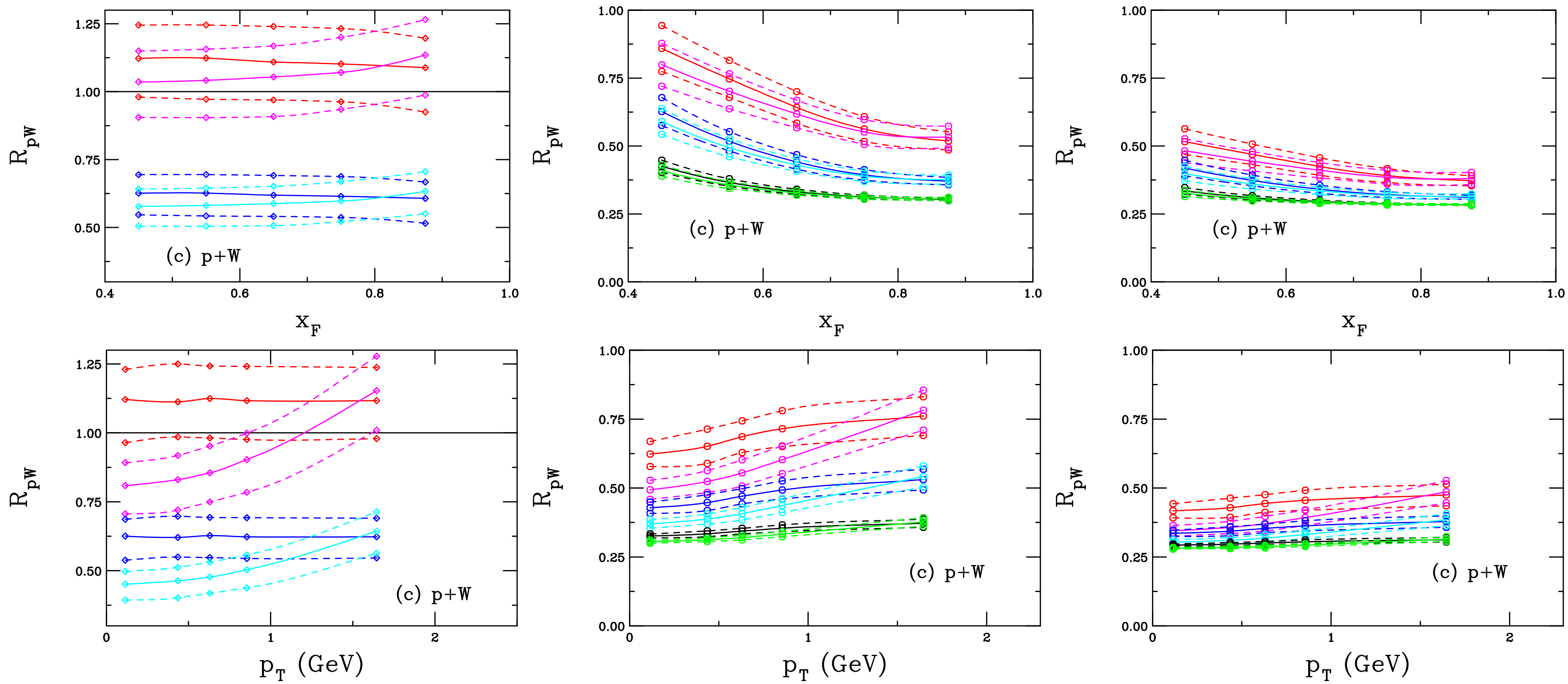

Figure 17: Left: no IC, red: EPPS16 only; magenta: EPPS16 + k_T broadening; blue and cyan, adding $\sigma_{\mathrm{abs}} = 9$ mb. Middle: solid lines: EPPS16 + IC; dashed: including k_T broadening; $P^0_{\mathrm{ic},5} = 0.1\%$ (red, magenta), 0.31% (blue, cyan), 1% (green, black). Right: Same as middle but with $\sigma_{\mathrm{abs}} = 9$ mb

SMOG J/ψ Results Compared to Calculations

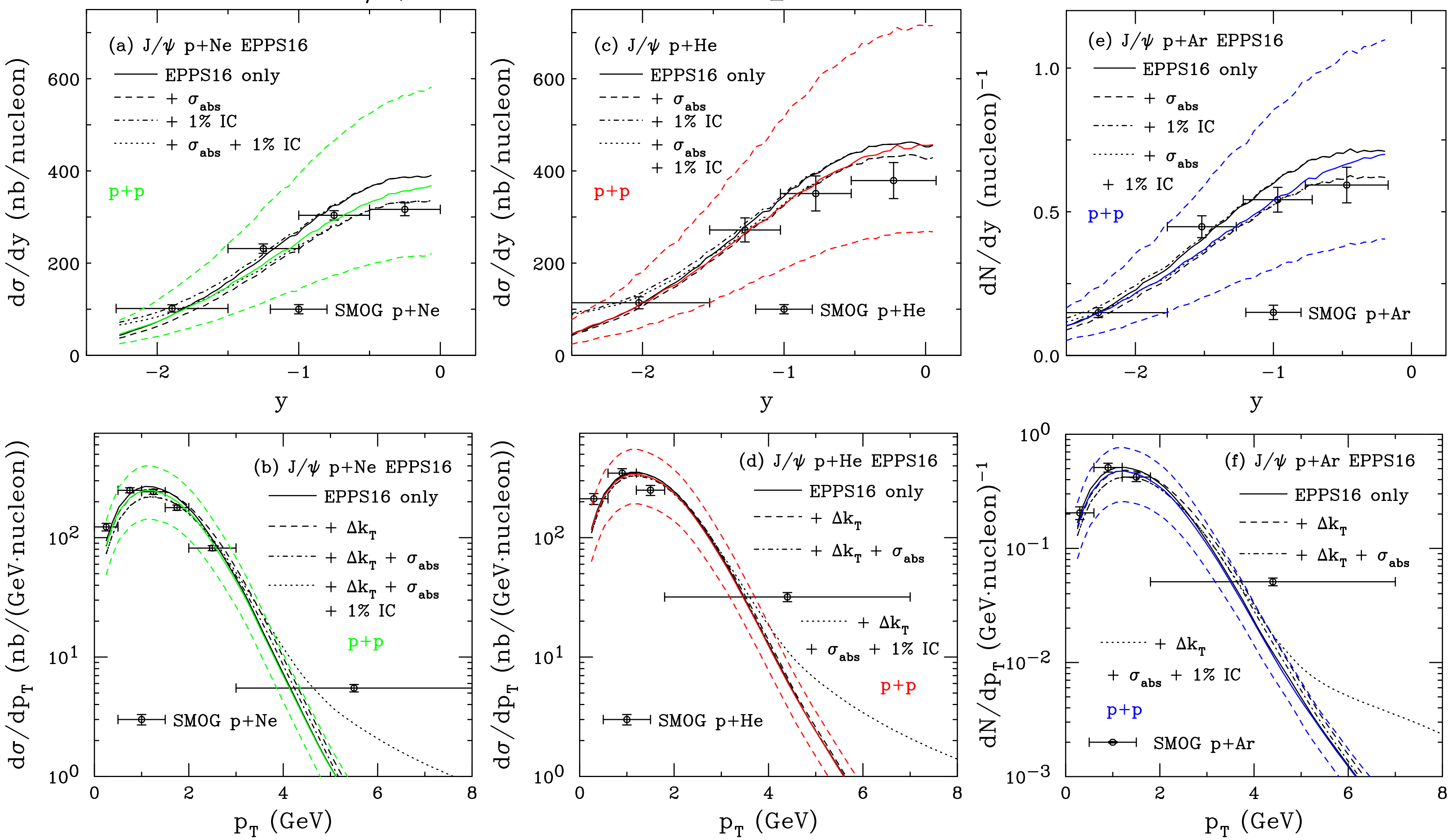

Figure 18: The J/ψ cross section as a function of y in (a), (c), (e) and p_T in (b), (d), (f) for p+Ne ($\sqrt{s_{NN}} = 68.5$ GeV) in (a) and (b); p+He ($\sqrt{s_{NN}} = 86.6$ GeV) in (c) and (d); and $p+$Ar ($\sqrt{s_{NN}} = 110.4$ GeV) in (e) and (f). The black curves are the $p+A$ calculations. The colored curves (solid and dashed) show the CEM $p+p$ calculations (no IC). The $p+A$ rapidity distributions are shown for EPPS16 only (solid); EPPS16 with absorption (dashed); EPPS16 and $P^0_{\rm ic\,5} = 1\%$ (dot-dashed); and EPPS16, absorption, and $P^0_{\rm ic\,5} = 1\%$ (dotted). The p_T distributions show EPPS16 only (solid); EPPS16 with k_T kick (dashed); EPPS16, absorption, and k_T kick (dot-dashed); and EPPS16, absorption, k_T kick and $P^0_{\rm ic\,5} = 1\%$ (dotted). The $p+$Ne data are from arXiv:2211.11645; the $p+$He and $p+$Ar data are from PRL **122**, 132002 (2019).

Summary

aSeveral different approaches to absorption

J/ψ and ψ' nuclear effects measured at different energies, also Υ family measured in fixed target interactions by E772

Absorption assumed ineffective at the LHC

Shadowing studied with absorption at RHIC as a function of centrality, seems indicative of a hot spot where shadowing was effective

Comover interactions give similar A dependence as absorption but has survived by adapting comovers to be either gluons (in QGP) or hadrons (in hadronic media)

Intrinsic charm is good agreement with data on charm production